Radiol Phys Technol (2017) 10:60–67
DOI 10.1007/s12194-016-0368-z

Dose reduction technique in diagnostic X-ray computed tomography by use of 6-channel multileaf collimators

Fumio Hashimoto[1] · Atsushi Teramoto[1] · Yasuki Asada[1] · Shoichi Suzuki[1] · Hiroshi Fujita[2]

Received: 16 March 2016 / Revised: 27 June 2016 / Accepted: 30 June 2016 / Published online: 9 July 2016

Abstract Recently, region-setting computed tomography (CT) has been studied as a region of interest imaging method. This technique can strongly reduce the radiation dose by limiting the irradiation field. Although mathematical studies have been performed for reduction of the truncation artifact, no experimental studies have been performed so far. In this study, we developed a three-dimensional region-setting CT system and evaluated its imaging properties. As an experimental system, we developed an X-ray CT system with multileaf collimators. In this system, truncated projection data can be captured by limiting of the radiation field. In addition, a truncated projection data correction was performed. Finally, image reconstruction was performed by use of the Feldkamp–Davis–Kress algorithm. In the experiments, the line profiles and the image quality of the reconstructed images were evaluated. The results suggested that the image quality of the proposed method is comparable to that of the original method. Furthermore, we confirmed that the radiation dose was reduced when this system was used. These results indicate that a 3D region-setting CT system using 6-channel multileaf collimators can reduce the radiation dose without in causing a degradation of image quality.

Keywords Computed tomography · Radiation exposure · Image reconstruction · Truncated projection · Collimator

✉ Fumio Hashimoto
230.hashimoto@gmail.com

[1] Graduate School of Health Sciences, Fujita Health University, 1-98 Dengakugakubo, Kutsukake-cho, Toyoake, Aichi 470-1192, Japan

[2] Graduate School of Medicine, Gifu University, Gifu, Japan

1 Introduction

1.1 Background

Due to developments in computed tomography (CT) systems and the increase of CT examinations, CT examinations are of particular interest as a source of radiation exposure [1, 2]. However, CT examinations may increase the risk of cancer [3–5]. Therefore, many studies have been performed to reduce the radiation exposure level during CT examinations [6–12]. In the current diagnostic CT systems, an X-ray beam irradiates the entire field of view (FOV), even if we want to acquire only the region of interest (ROI). If a reconstructed image can be obtained for the truncated projection data by limiting of the irradiation field, the radiation dose can be strongly reduced. In this study, this mechanism is referred to as region-setting CT: an ROI imaging method.

1.2 Related works

In a prior study, Noo et al. [10] proposed an image reconstruction algorithm based on the Hilbert transform for truncated projection data. Kudo et al. [11] indicated that a priori knowledge of the reconstructed image in the ROI solves the interior problem [13], one of the inverse problems. Gong et al. [12] implemented interior micro-CT for achieving a lower radiation dose. Their system can acquire truncated projection data by using a fixed size collimator. We developed two-dimensional region-setting CT that supports ROIs of arbitrary shape [14]. To the best of our knowledge, there has been no study on the development of a three-dimensional (3D) experimental system for region-setting CT.

1.3 Objective

If multileaf collimators used during radiation therapy apply a diagnostic CT, there is the possibility that the radiation dose to organs at risk can be reduced. Our aim in this study was to develop a 3D region-setting CT system by use of multileaf collimators. In this paper, we analyze the results obtained using the experimental system, and we evaluate that system.

2 Materials and methods

2.1 Experimental system

2.1.1 Overview of the experimental system

A schematic of the region-setting CT system is shown in Fig. 1. This system comprises two parts: a scan part and a control part. The former consists of an X-ray tube (L7901, HAMAMATSU Photonics), a detector (C7942CA, HAMAMATSU Photonics), a multileaf collimators, etc., whereas the latter is connected to a motor control unit, X-ray control unit, image interface, and executed CT scan control and data transfer. The maximum tube voltage and current of the X-ray tube is 100 kV and 0.1 mA, respectively. The focus size is 5 μm, and the angle of the fan beam and cone beam is 2.9°. W and Be is introduced as target and window, respectively, and 0.5 mm Al is attached as a filter. As a detector, an indirect-conversion type flat-panel detector is adopted. The scintillator of the detector is CsI (Tl). The sensor pitch and matrix size is 50 μm and 2366 × 2368, respectively. The bit depth is 12 bit (1024), and frame rate is 2 frames per second. The computer controls the scan system from outside the X-ray shielded room.

In the CT system, projection data for all directions are collected by rotating the subject using a rotation stage. The rotation stage consists of a rotation table mounted with a step motor (DG130R-ASBA, ORIENTAL MOTOR Co., Ltd.), motor driver, and motion controller. The motion controller built in the computer transmits pulse trains to the motor driver. Then, the motor driver gives instructions to the step motor. The rotation speed and angle resolution is 200 rpm and 0.02°, respectively.

Considering the geometry of the system, the source-image receptor distance (SID) can be set as 510 mm, whereas the source-object distance (SOD) can be set from 200 to 450 mm.

2.1.2 Multileaf collimators

The experimental system shields the outside ROI by using multileaf collimators and collects the truncated projection data. A schematic for the multileaf collimators is shown in Fig. 2. The source–collimator distance is 100 mm, and a 6-channel Pb-leaf is controlled independently by use of servo motors (HS-785HB, Hitec Multiplex). Illustration of the system geometry is shown in Fig. 3. The Pb-leaf is controlled until the straight line connecting the X-ray tube focus and the outline of the ROI.

The operating speed of the Pb-leaf is 2.17 mm/s, and the mechanical errors of the Pb-leaf are within ±0.7 mm. These control programs are developed by use of Visual C++ 6.0 (Microsoft Corporation).

2.2 Image reconstruction

A flowchart of the image reconstruction process is shown in Fig. 4. In our imaging system, truncation artifacts occur in the reconstructed images if the truncated projection data are obtained directly. To reduce truncation artifacts, we performed truncated projection data correction and image reconstruction.

2.2.1 Truncated projection data correction

The data correction process for truncated projection data consists of extension and extrapolation of the projection data. A diagrammatic representation of the data correction

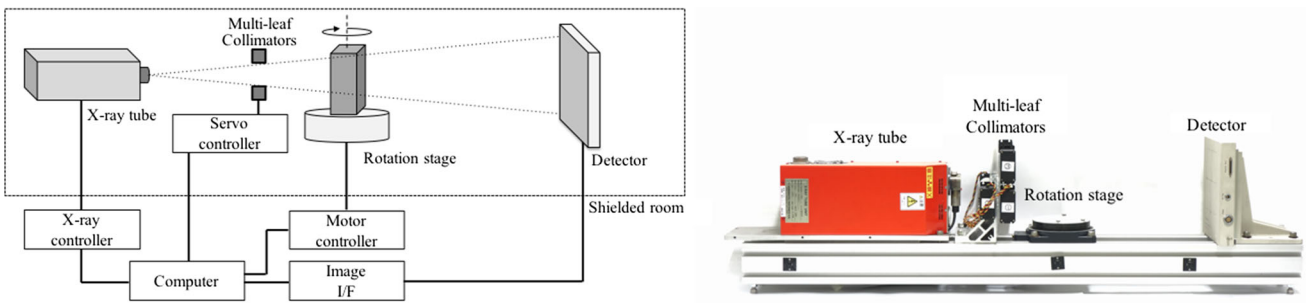

Fig. 1 Schematic for the region-setting CT system

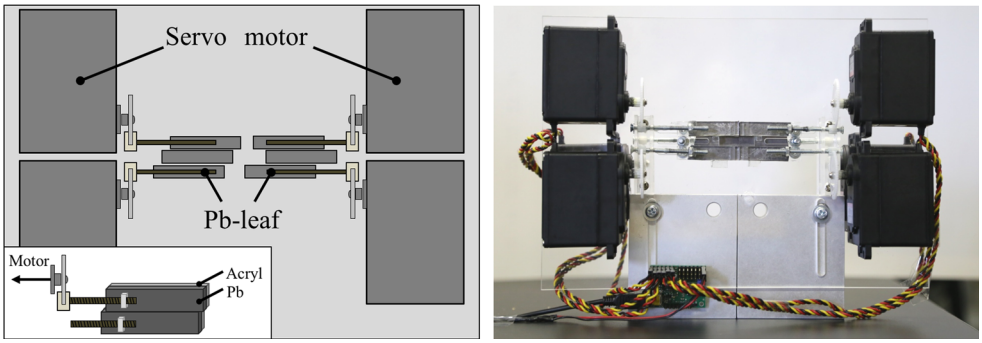

Fig. 2 Schematic for the multileaf collimators

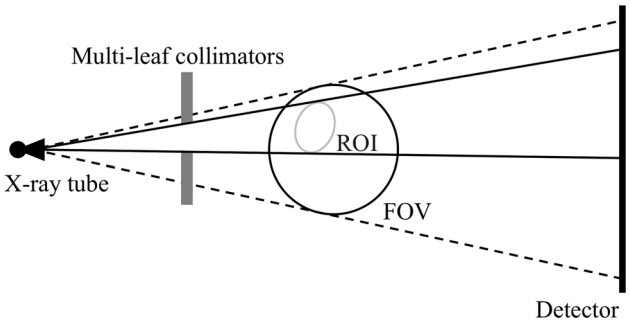

Fig. 3 Illustration of the structure of the Pb-leaf. The Pb-leaf is controlled until the straight line connecting the X-ray tube focus and the outline of the ROI

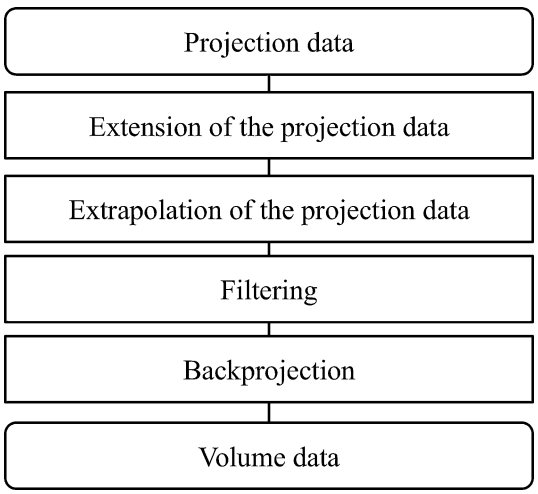

Fig. 4 Flowchart of the image reconstruction process

is shown in Fig. 5. The horizontal direction of the raw projection data is extended, as shown in Fig. 5a and b. Then, the projection data are extrapolated truncated area (Fig. 5c). The data correction details are explained in the following.

2.2.1.1 Extension of the projection data For extension of the projection data, the extrapolating area is reserved. Two-dimensional projection data $p(u,v)$ are extended in the horizontal direction, and extended projection data $p'(u',v)$ are obtained.

Here, u and v are the spatial coordinates of the detector (horizontally, vertically), and u' is the horizontal spatial coordinate of the extended projection data. A schematic diagram for the extended projection data is shown in Fig. 6.

2.2.1.2 Extrapolation of the projection data For extrapolation of the projection data, the projection data $p'(u',v)$ are extrapolated along the horizontal direction of the data based on the cosine function. Let us denote the extrapolated distance by $W_l(v)$, $W_r(v)$, and the horizontal spatial coordinates of the truncated boundary by $k_l(v)$, $k_r(v)$.

First, W_l and W_r are calculated from coordinates at k_l and k_r and the left and right end parts of the projection data p', respectively. Then, the projection data are extrapolated from k_l, k_r toward the end parts of the data based on the cosine function.The extrapolation equation is defined as follows:

$$q(u',v) = \begin{cases} p'(k_l(v),v) \cdot \cos^2\left(\dfrac{\pi(k_l(v)-u')}{2W_l(v)}\right) & k_l(v) > u' \\ p'(k_r(v),v) \cdot \cos^2\left(\dfrac{\pi(k_r(v)-u')}{2W_r(v)}\right) & k_r(v) < u' \end{cases}, \quad (1)$$

where $q(u',v)$ is the extrapolated projection data. A schematic diagram for the extrapolated projection data is shown in Fig. 7.

By application of processing, the error of the signal at the truncated boundary can be reduced. Therefore, truncation artifacts caused by the reconstruction filtering can be suppressed.

2.2.2 Image reconstruction

As an image reconstruction algorithm, the Feldkamp–Davis–Kress (FDK) algorithm [15, 16] is introduced. In addition, the Ramachandran–Lakshminarayanan filter is

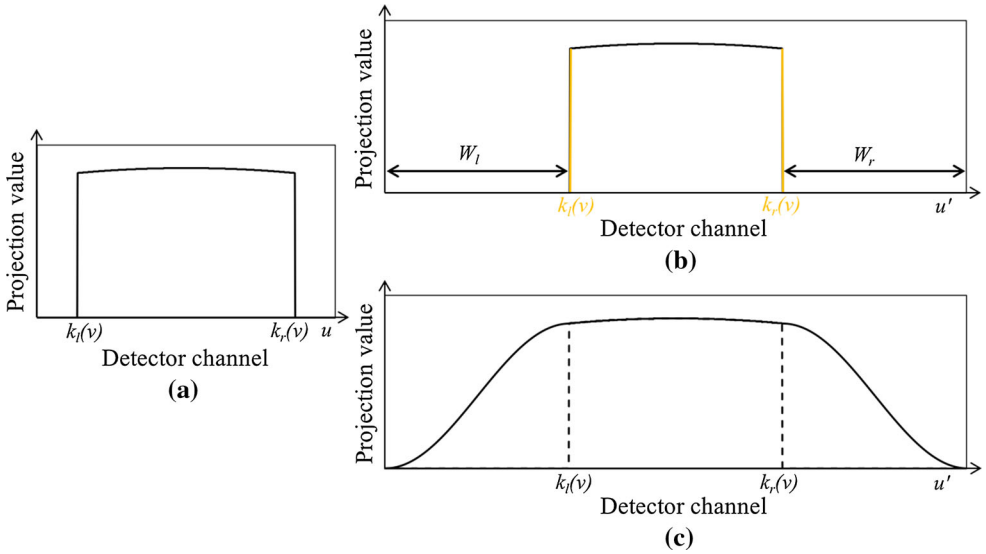

Fig. 5 Outline of the correction of the truncated projection data. **a** Raw projection data. **b** Extended projection data. **c** Extrapolated projection data

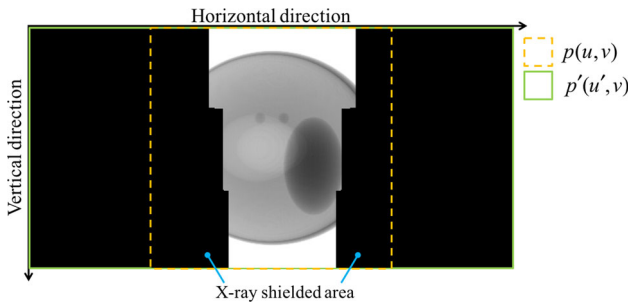

Fig. 6 Schematic diagram for the extended projection data. The *black region* of $p(u,v)$ is shielded by the multileaf collimators

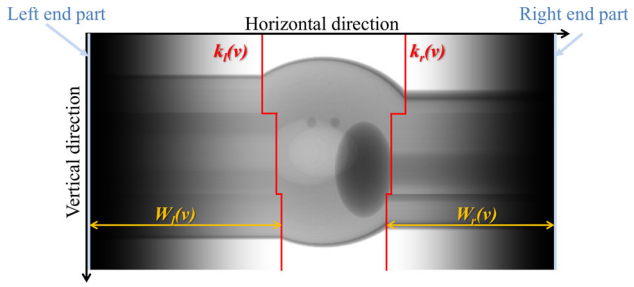

Fig. 7 Schematic diagram for the extrapolated projection data

introduced as a reconstruction filter. This program is developed by use of Visual C++ 2012 (Microsoft Corporation) and an Intel C++ compiler (Intel Corporation). Furthermore, the program performs parallel processing by using a multi-core processor (Intel Core i5-3470, 3.20 GHz).

2.3 Performance evaluation

Both original and region-setting CT scans of two customized phantoms were conducted for image and radiation dose evaluations. The original method acquired non-truncated projection data without multileaf collimators and was employed as the baseline for the evaluations. For the purpose of comparison, we evaluated three methods. First, we compared the uncorrected method obtained directly using the truncated projection data. Second, we compared the mean value substitution (MVS) method [14] and finally the proposed method. Tube voltage and current of the experiment were set to 80 kV and 0.1 mA, respectively. The number of projection was 360; our CT system acquired using step and shoot technique.

2.3.1 Evaluation using image evaluation phantom

Line profile and quantitative evaluations were performed with use of an image evaluation phantom for evaluation of the image quality of the system. The image evaluation phantom is shown in Fig. 8. This phantom consists of a cylindrical ABS resin container and three rods (ABS resin, acrylic resin, and aluminum). The diameters of the container and rods were 30 and 5 mm, respectively. The exposure time per projection was 1.0 s.

We set the ROI shape to a sphere and an ellipsoid. Three quantitative metrics were measured, including the correlation coefficient (CC), mean absolute error (MAE), and normalized mean square error (NMSE) [17]. The MAE and NMSE were calculated using of the following equation:

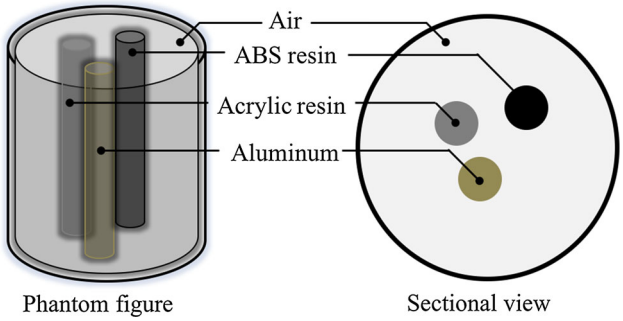

Fig. 8 Schematic of the image evaluation phantom

$$MAE = \frac{1}{N}\sum_{i\in R}|f'(i) - f(i)|, \tag{2}$$

$$NMSE = \frac{\sum_{i\in R}\{f'(i) - f(i)\}^2}{\sum_{i\in R} f(i)^2}, \tag{3}$$

where $f(i)$ and $f'(i)$ indicate the baseline image and the target image, respectively. Region R indicates the ROI. N is the number of voxels in region R. If the target image was exactly the same as the baseline image, the MAE and NMSE would be 0.

2.3.2 Evaluation with use of chest phantom

To verify the effectiveness of the experimental system, we designed and scanned a tiny chest phantom. The illustration of the chest phantom is shown in Fig. 9. This phantom is made of acrylic resin and consists of lung, cardiac, and vertebral regions. A bone-equivalent material (dipotassium hydrogen phosphate, CT value = 500 HU) is filled in the vertebral region. The exposure time per projection was 1.0 s, and we set the ROI on a cardiac region. In addition, the air kerma in the chest phantom were evaluated with a thermoluminescent dosimeter (TLD) (MSO-S, Kyokko). The TLDs were annealed using an annealing oven (AO-SL, Kyokko) at 450 °C for 20 min. After measurements, the TLDs were read immediately on the TLD reader (3000, Kyokko). Finally, the air kermas were calculated by multiplying of the measured TLD value and conversion factor of each dosimeter. Here, the conversion factors (mGy/mSv) were calculated by division of the TLD value by the air kerma measured with an ionization chamber dosimeter (9015, Radcal). The exposure time was set to 180 s.

3 Results

3.1 Image evaluation

The reconstructed images of the image evaluation phantom and the volume-rendered images are shown in Figs. 10 and 11, respectively. Figure 10 shows an axial section of the image evaluation phantom. With the proposed method, artifacts were not found in the peripheral region. The line profiles are plotted in Fig. 12. The line profile selection is shown by the yellow line of Fig. 10a. Regarding shape similarity of the profile between two ROI imaging methods and original method, the similarity of the proposed method was better than that of the uncorrected method.

The reconstruction images of the chest phantom are shown in Fig. 13. In the proposed method, the 3D ROI images were clearly identified; however, artifacts are found in the peripheral region of the images obtained.

Quantitative evaluation results for the image quality phantom are shown in Table 1. In the evaluation, three methods (uncorrected, proposed, and MVS methods) were evaluated. The proposed methods were found to have a strong correlation. The MAE and NMSE in the spherical

Fig. 9 Schematic of the tiny chest phantom

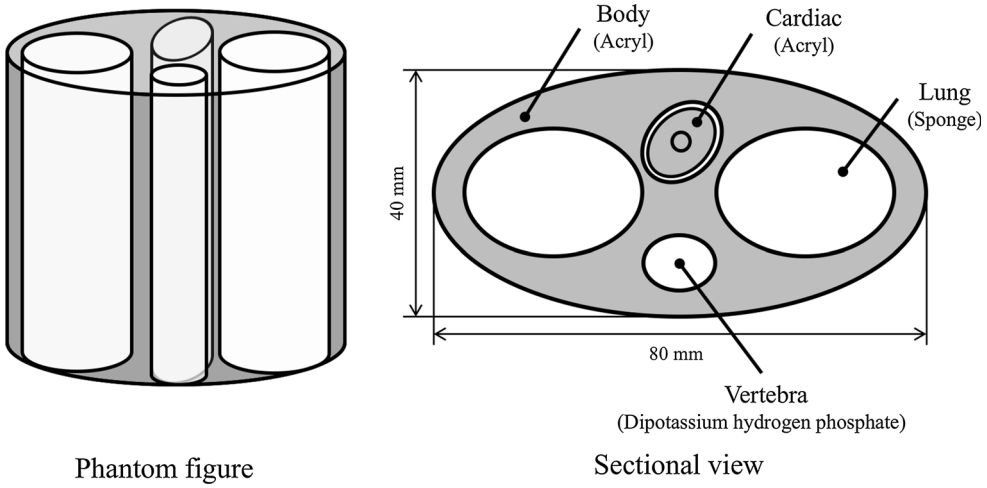

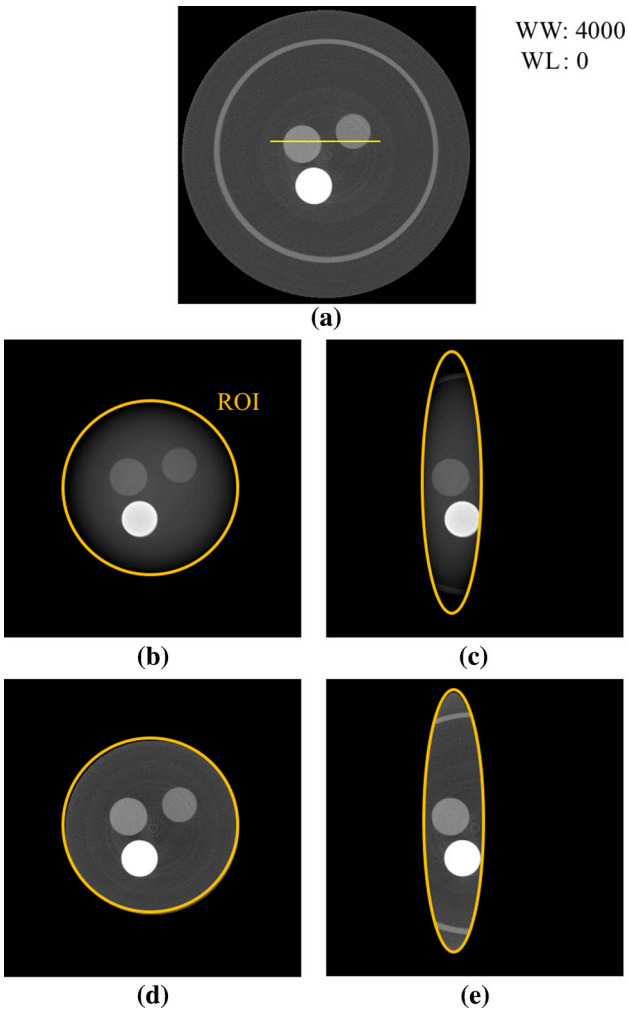

Fig. 10 Reconstructed images of the image quality phantom. **a** Original method and line profile selection. **b** Uncorrected method (ROI: *sphere*). **c** Uncorrected method (ROI: *ellipsoid*). **d** Proposed method (ROI: *sphere*). **e** Proposed method (ROI: *ellipsoid*)

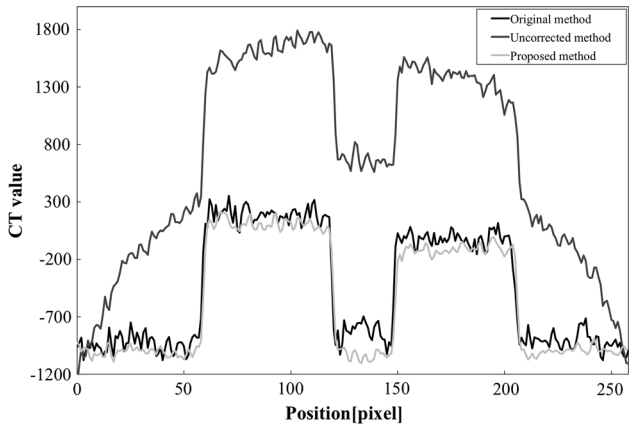

Fig. 12 Line profiles of the reconstructed images of the image quality phantom

ROI were reduced to 1/8 and 1/32, respectively, by the truncated projection data correction as compared to the uncorrected method. The MAE and NMSE in the ellipsoidal ROI were also reduced to 1/5 and 1/9, respectively.

3.2 Radiation dose

The results of the radiation dose measurements are shown in Table 2. The proposed method reduced the radiation dose for the lung region by 80 % as compared to the original method.

4 Discussion

We have presented a dose reduction technique in X-ray CT by use of multileaf collimators.

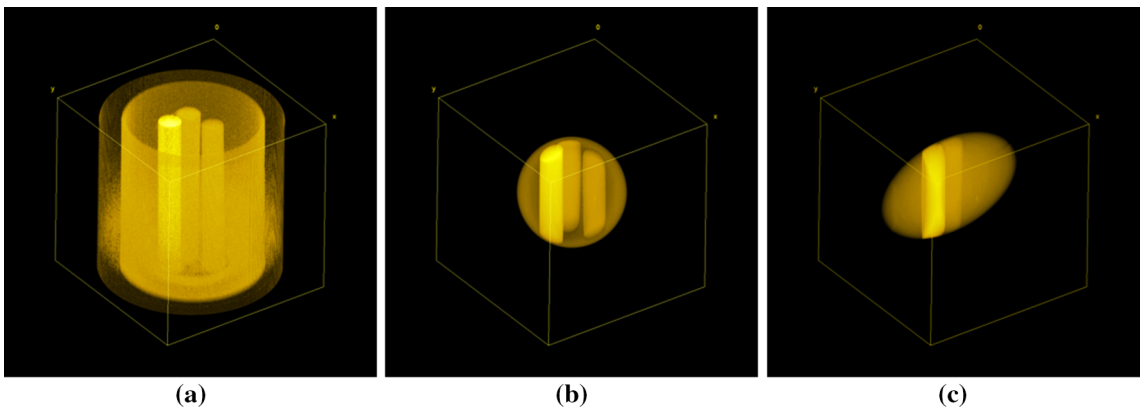

Fig. 11 Volume-rendered images of the image quality phantom. **a** Original method. **b** Proposed method (ROI: *sphere*). **c** Proposed method (ROI: *ellipsoid*)

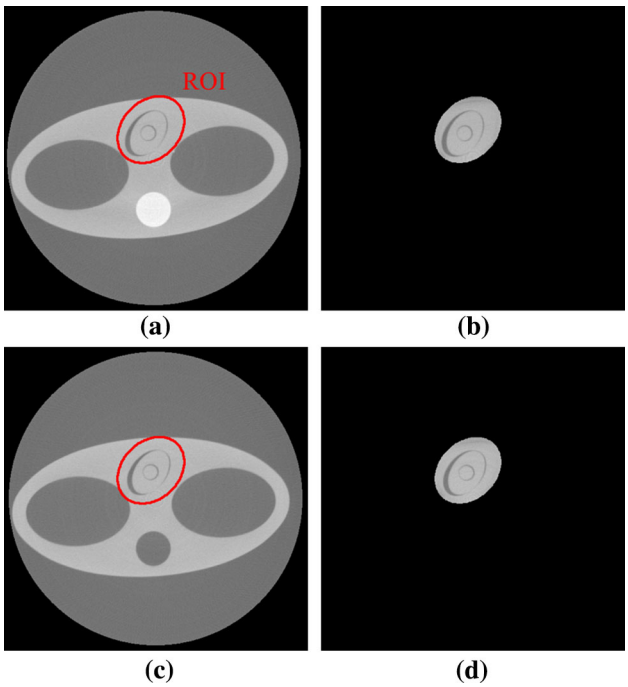

Fig. 13 Reconstructed images of the chest phantom. **a** Original method with bone. **b** Proposed method with bone. **c** Original method without bone. **d** Proposed method without bone

As shown from the line profiles, the uncorrected method was considerably different from that obtained using the original method. On the other hand, the profile of the proposed method was similar to that obtained using the original method. In the proposed method, the MAE and NMSE in the spherical ROI were reduced to 1/8 and 1/32, respectively, as compared to the uncorrected method. The MAE and NMSE in the ellipsoidal ROI were also reduced to 1/5 and 1/9, respectively. Furthermore, the MAE and NMSE were reduced compared with the MVS method. These improvements are due to the reduction of truncation artifacts. Because the signal edge at the truncated projection data was attenuated gradually, it is likely to suppress the truncation artifacts. These results indicate that our proposed system can set the ROI to any shape. It also suggests that the image quality of the proposed method is similar to that of the original method. In addition, by using the proposed method, we can obtain ROI images without a priori knowledge of the reconstructed image in the ROI, which is required by existing methods [10, 11]. Furthermore, the proposed method does not use parallel beam reconstruction as used in previous research, but uses cone beam reconstruction [10, 11]. Thus, our proposed method is more practical than existing methods.

Table 2 Radiation dose results of the chest phantom

Organs	Original method ($n = 2$)		Proposed method ($n = 3$)	
	Average	SD	Average	SD
Cardiac	18.4	0.93	14.4	2.11
Lung (left)	18.3	1.23	3.79	0.60
Lung (right)	16.2	0.21	3.79	0.17

Units in mGy

In the tiny chest phantom, as compared to the uncorrected method, our proposed method provided favorable reconstructed images. However, artifacts appeared in the peripheral region of the images. In the experimental system, the X-ray beam is shielded by the multileaf collimators, and this causes scattering from the Pb-leaf of the multileaf collimators. Further studies need to be performed a design of collimators for the suppression of scattering.

In the radiation dose measurements, the air kerma of the lung region was reduced to a maximum of 80 %, whereas the air kerma of the cardiac region was reduced to 79 % by lower scattering because of the limited X-ray beam. These results indicate that 3D region-setting CT system using 6-channel multileaf collimators can reduce the radiation dose without in causing a degradation of image quality.

5 Limitation

This study is restricted to an experimental system. The differences between the geometry of the system are likely to result in artifacts from scattering. In addition, this study is a phantom study. In the future, we need to examine a biological sample such as a human body. Future work involves validation for diagnostic CT systems. In addition, we will need to evaluate image contrast, spatial resolution, and noise.

Table 1 Quantitative evaluation results for the image quality phantom datasets

	Sphere			Ellipsoid		
	Uncorrected method	MVS method	Proposed method	Uncorrected method	MVS method	Proposed method
Correlation coefficient	0.995	0.999	0.999	0.999	0.998	0.999
MAE [HU]	1027.0	171.5	130.5	841.2	204.0	165.9
NMSE	0.66	0.04	0.02	0.37	0.05	0.04

6 Conclusion

We have developed a dose reduction technique for diagnostic CT by using multileaf collimators. In addition, we evaluated the image quality and radiation dose of the proposed method. We found that the image quality of the proposed method is similar to that of the original method. Furthermore, we confirmed that the radiation dose was reduced in this system. These results indicate that 3D region-setting CT system using 6-channel multileaf collimators can reduce the radiation dose without in causing a degradation of image quality.

Acknowledgments I would like to show my greatest appreciation to Chika Murata, whose comments and suggestions were of inestimable value for my study. This manuscript was presented orally at the 71st Annual meeting of the Japanese Society of Radiological Technology.

Compliances with ethical standards

Conflict of interest The authors declare that they have no conflict of interest.

References

1. UNSCEAR 2008 report. Vol. I: sources of ionizing radiation. Annex A: medical radiation exposures. 2010. http://www.unscear.org/docs/reports/2008/09-86753_Report_2008_Annex_A.pdf. Accessed 14 Mar 2016.
2. Asada Y, Suzuki S, Kobayashi K, Kato H. Investigation of patient exposure doses in diagnostic radiography in 2011 questionnaire. Nihon Hoshasen Gijutsu Gakkai Zasshi. 2013;69:371–9.
3. de González A, Darby S. Risk of cancer from diagnostic X-rays: estimates for the UK and 14 other countries. Lancet. 2004;363:345–51.
4. Brenner D, Hall E. Computed tomography—an increasing source of radiation exposure. N Engl J Med. 2007;357:2277–84.
5. Nguyen P, Lee W, Li Y, Hong W. Assessment of the radiation effects of cardiac CT angiography using protein and genetic biomarkers. JACC Cardiovasc Imaging. 2015;8:873–84.
6. Silva A, Lawder H, Hara A. Innovations in CT dose reduction strategy: application of the adaptive statistical iterative reconstruction algorithm. AJR Am J Roentgenol. 2010;194:191–9.
7. Xia Y, Dennerlein F, Bauer S. Scaling calibration in region of interest reconstruction with the 1D and 2D ATRACT algorithm. Int J Comput Assist Radiol Surg. 2014;9:345–56.
8. Seger MM. Rampfilter implementation on truncated projection data. Application to 3D linear tomography for logs. In: proc. SSAB02 symp. image anal. 2002. p. 33–36.
9. Ohnesorge B, Flohr T, Schwarz K, Heiken J, Bae K. Efficient correction for CT image artifacts caused by objects extending outside the scan field of view. Med Phys. 2000;27:39–46.
10. Noo F, Clackdoyle R, Pack J. A two-step Hilbert transform method for 2D image reconstruction. Phys Med Biol. 2004;49:3903–23.
11. Kudo H, Courdurier M, Noo F, Defrise M. Tiny a priori knowledge solves the interior problem in computed tomography. Phys Med Biol. 2008;53:2207–31.
12. Gong H, Lu J, Zhou O, Cao G. Implementation of interior micro-CT on a carbon nanotube dynamic micro-CT scanner for lower radiation dose. In: proc SPIE med. imaging. int. soc. opt. photonics. 2015. p. 94124N–94124N–9.
13. Natterer F. The mathematics of computerized tomography. New York: Siam; 1986. p. 158–79.
14. Hashimoto F, Teramoto A, Asada Y, Suzuki S, Fujita H. Development of the two-dimensional region-setting CT system: development and basic evaluation of the experimental system using the active collimators. Med Imaging Technol. 2016;34:123–7.
15. Shepp L, Kruskal J. Computerized tomography: the new medical X-ray technology. Am Math Mon. 1978;85:420–39.
16. Feldkamp L, Davis L, Kress J. Practical cone-beam algorithm. J Opt Soc Am A. 1984;1:612–9.
17. Penney BC. Constrained least-squares restoration of nuclear medicine images: selecting the coarseness function. Med Phys. 1987;14:849–58.